Remote Sensing of Environment 113 (2009) 2606–2617

Contents lists available at ScienceDirect

Remote Sensing of Environment

journal homepage: www.elsevier.com/locate/rse

Spatial–temporal dynamics of land surface temperature in relation to fractional vegetation cover and land use/cover in the Tabriz urban area, Iran

Reza Amiri [a], Qihao Weng [b,*], Abbas Alimohammadi [c], Seyed Kazem Alavipanah [d]

[a] School of Geography and Environmental Science, Monash University, Clayton, Victoria 3800, Australia
[b] Center for Urban and Environmental Change, Department of Geography, Geology, and Anthropology, Indiana State University, Terre Haute, IN 47809, USA
[c] Department of GIS, K. N. Toosi University of Technology, Tehran, Iran
[d] Department of Cartography, Faculty of Geography, University of Tehran, Tehran, Iran

ARTICLE INFO

Article history:
Received 6 October 2008
Received in revised form 22 July 2009
Accepted 23 July 2009

Keywords:
Land surface temperature
Vegetation cover
TVX space
LULC change
Urban

ABSTRACT

Rapid changes of land use and land cover (LULC) in urban areas have become a major environmental concern due to environmental impacts, such as the reduction of green spaces and development of urban heat islands (UHI). Monitoring and management plans are required to solve this problem effectively. The Tabriz metropolitan area in Iran, selected as a case study for this research, is an example of a fast growing city. Multi-temporal images acquired by Landsat 4, 5 TM and Landsat 7 ETM+ sensors on 30 June 1989, 18 August 1998, and 2 August 2001 respectively, were corrected for radiometric and geometric errors, and processed to extract LULC classes and land surface temperature (LST). The relationship between temporal dynamics of LST and LULC was then examined. The temperature vegetation index (TVX) space was constructed in order to study the temporal variability of thermal data and vegetation cover. Temporal trajectory of pixels in the TVX space showed that most changes due to urbanization were observable as the pixels migrated from the low temperature-dense vegetation condition to the high temperature-sparse vegetation condition in the TVX space. The uncertainty analysis revealed that the trajectory analysis in the TVX space involved a class-dependant noise component. This emphasized the need for multiple LULC control points in the TVX space. In addition, this research suggests that the use of multi-temporal satellite data together with the examination of changes in the TVX space is effective and useful in urban LULC change monitoring and analysis of urban surface temperature conditions as long as the uncertainty is addressed.

1. Introduction

Since Rao (1972) first showed the possibility of detecting the thermal footprint of urban areas in satellite images, a wide range of satellite and airborne sensors has been used to study land surface temperature (LST) and urban heat island (UHI) by offering enhancement over their predecessors (e.g. Streutker, 2003; Weng, 2001; Weng et al., 2004; Nichol, 2005; Pongracz et al., 2006). Land surface temperature observations acquired by remote sensing technologies have been used to assess the UHI, to develop models of land surface–atmosphere exchange, and to analyze the relationship between temperature and land use and land cover (LULC) in urban areas (Voogt & Oke, 2003). Recent studies have addressed the relationship between LST and surface characteristics such as vegetation indices (e.g. Carlson et al., 1994; Owen et al., 1998). Some studies investigated the effect of biophysical factors on LST by making use of fundamental surface descriptors such as vegetation fraction instead of qualitative LULC classes (Gallo &Tarpley, 1996; Owen et al., 1998; Dousset & Gourmelon, 2003). The vegetation index–LST relationship has been used by Carlson et al. (1994) to retrieve surface biophysical parameters, by Kustas et al. (2003) to extract sub-pixel thermal variations, and by Lambin and Ehrlich (1996) to analyze land cover dynamics. Many investigators have observed a negative relationship between vegetation index and LST. This finding stimulated further research into two major pathways, namely, statistical analysis of the relationship and the temperature/vegetation index (TVX) approach. TVX by definition is a multi-spectral method of combining LST and a vegetation index (VI) in a scatterplot to observe their associations (Quattrochi & Luvall, 2004).

During the past few decades, different variations of the TVX approach to the LST–vegetation abundance relationship have been developed. Price (1990) found that radiant surface temperature showed more variation in sparsely vegetated areas than in densely vegetated areas. This behavior results in the typical triangular or, as observed by Moran et al. (1994), trapezoidal shape for large heterogeneous regions under strongly sunlit conditions (Gillies et al., 1997). These early works have stimulated the development of different applications of the TVX concept. Ridd (1995) and Carlson et al. (1994) interpreted different

* Corresponding author. Tel.: +1 812 237 2255; fax: +1 812 237 8029.
E-mail addresses: reza.amiri@arts.monash.edu.au (R. Amiri), qweng@indstate.edu (Q. Weng), alimoh_abb@kntu.ac.ir (A. Alimohammadi), salavipa@ut.ac.ir (S.K. Alavipanah).

0034-4257/$ – see front matter © 2009 Elsevier Inc. All rights reserved.
doi:10.1016/j.rse.2009.07.021

sections of the triangle and related them to different LULC types. Lambin and Ehrlich (1996) presented a comprehensive interpretation of the TVX space, and Carlson and Arthur (2000) interpreted the physical meaning of the space. Further, Goward et al. (2002) gave a detailed analysis of the underlying biophysics of the observed TVX relationship and suggested that the relationship was the result of a modulation of radiant surface temperature by vegetation cover.

The TVX approach has been the subject of multiple studies focusing on the development of new applications, which used different vegetation types at different scales from local to global. Researchers used the TVX concept to develop new indices (e.g. Moran et al., 1994; Lambin & Ehrlich, 1996; Owen et al., 1998; Carlson & Arthur, 2000; Sandholt et al., 2002; Chen et al., 2006) and to estimate surface parameters (e.g. Moran et al., 1994; Jiang & Islam, 2001; Nishida et al., 2003; Carlson, 2007). Nishida et al. (2003) discussed major difficulties of the TVX method for evapotranspiration (ET) estimation and suggested a model for urbanization monitoring as ET was able to capture variations in surface energy partitioning. Apart from the introduction of new indices and surface parameters estimation, considerable research has been carried out on the extraction of new TVX metrics by focusing on the LST-NDVI fit line (Nemani & Running, 1989; Smith & Choudhury, 1991) and by interpreting the variations in the characteristics of TVX correlation in relation to surface parameters such as stomatal resistance and the evapotranspiration rate (Nemani & Running, 1989; Sandholt et al., 2002). The TVX approach has further been used in the so-called "Triangle Method" to derive surface parameters. The "Triangle Method" is used by Carlson et al. (1994) to extract soil moisture content and fractional vegetation cover (Fr), by Goward et al. (2002) to assess soil moisture condition and by Owen et al. (1998) to assess the impact of urbanization on these parameters. Recently, Carlson (2007) provided a comprehensive review of the "Triangle Method" for the estimation of evapotranspiration and soil moisture.

Finally, the TVX concept has been used to perform pixel trajectories. This idea has emerged over the past decade that land surface parameters associated with individual pixels can be visualized as vectors tracing out paths in multi-parameter space (Lambin & Ehrlich, 1996). Several studies verified that urbanization was the major cause of the observed migration of pixels within the multi-temporal TVX space (Owen et al., 1998; Carlson & Sanchez-Azofeifa, 1999). Owen et al. (1998) found that the initial location of the migrating pixels in the TVX triangle determined the magnitude and direction of the path. Carlson and Sanches-Azofeifa (1999) used the TVX method to assess how surface climate was affected by rapid urbanization and deforestation in San Jose, Costa Rica. They showed that urbanization was more effective than deforestation, and that different development styles followed different paths in the space. Carlson and Arthur (2000) also compared average trajectories of different development styles, and showed that in advanced stages of development, the paths became closer and undistinguishable. However, these studies do not provide a means for addressing the uncertainty in the TVX space. They also study the migration of pixels for different neighborhoods or development styles and the trajectory of migrating pixels due to LULC changes in the TVX space has not been addressed. Here we address these issues in a semi-arid urban area.

In this study, multi-temporal Landsat TM and ETM+ thermal and reflective data were used to study the spatial and temporal dynamics of LST in relation to a biophysical parameter (vegetation index) in the Tabriz semi-arid area of Iran, a fast growing urban area. This study is divided into two sections. First, the TVX method was used to normalize images for comparison and to perform pixel trajectory in the TVX space in order to observe the effect of changes in parameters due to urbanization related LULC changes. Secondly, the TVX method along with change vector analysis was applied to examine the relationship between the changes in LST/NDVI space and LULC classes and the uncertainty included in the TVX space. In addition, LULC changes under the rapid urbanization in Tabriz and the effects of these changes on surface thermal patterns were investigated.

2. Data and methodology

2.1. Study area

The city of Tabriz (38°05′, 46°17′), the capital of East Azerbaijan is in northwestern Iran (Fig. 1). The city is located at the eastern-most point of the triangular plain of Lake Urmia, which has an average elevation of 1300 m in a bowl-shaped valley, which is surrounded in all directions except the east and the north east by the steep foothill of mountain ranges. Tabriz experiences warm summers and cold winters, and has an average annual temperature of 12.2 °C. It has an annual precipitation of 311.1 mm, which falls mostly in winter and spring and accounts for almost half of annual potential evapotranspiration in this semiarid region. Due to the semiarid climate, bare soil is exposed between sparse vegetation cover. Dense vegetation coverage is limited to plains where surface water or ground water is available in the form of agricultural areas.

Since the second half of the 20th century, increasing migration and industrial development have accelerated population growth, which for a 50-year period (1956–2006) was ranked very high in the nation (Iran Census Center, 2007). Today, with a population of about 1.5 million, the city is a major center of culture, industry, commerce and transportation. As the biggest city in the western half of the country, Tabriz is selected for this study, exhibiting rapid population growth and urban expansion in the form of encroachment to the limited agricultural areas in limited directions at the cost of destruction of vegetation coverage. This study of LULC changes in connection with surface characteristics is important in integration of knowledge in decision-making process for future development of the city.

2.2. Data used and image pre-processing

Thermal IR images acquired by Landsat 4 and 5 TM and Landsat 7 ETM+ sensors of 30 June 1989, 18 August 1998, and 2 August 2001 respectively were used to extract LST data. Reflective data from these sensors were used to extract LULC classes. In addition to these data, digital topographic maps of 1:25,000 scales were used to correct the images for geometric errors and to define the extent of the city.

In order to reach an acceptable geometric accuracy, a multi-band image of 1998 was registered to topographic maps of the UTM coordinate system. This image was used as a reference image to register with the other images. The root-mean-square-error (RMSE) of 1989 and 2001 images was estimated to be 0.43 and 0.48 respectively. Because of the importance of linear features, a linear re-sampling method was used in order to preserve the linear details.

These images were suitable for multi-temporal studies because there was little difference in sun elevation and azimuth at the time of image acquisition at different dates. Application of a proper radiometric correction procedure is a necessary step for extracting reliable LULC classes and estimating LSTs. Because atmospheric properties at the times of image acquisitions were not available, multi-temporal image normalization using regression was used. Digital number (DN) values of the 2001 image were used as a base to the 1998 image and transformation functions were extracted for each band pair. This technique was also applied to the 1989 image. In order to remove the effect of cloud coverage and shadows in the classification and LST estimation, these regions were detected and masked out from the 1998 image by visual inspection and applying appropriate thresholds.

NDVI was used as an index of vegetation abundance. This index is related to biomass, chlorophyll content and water stress, and was calculated by using:

$$\mathrm{NDVI} = (\mathrm{NIR} - \mathrm{RED}) / (\mathrm{NIR} + \mathrm{RED}). \quad (1)$$

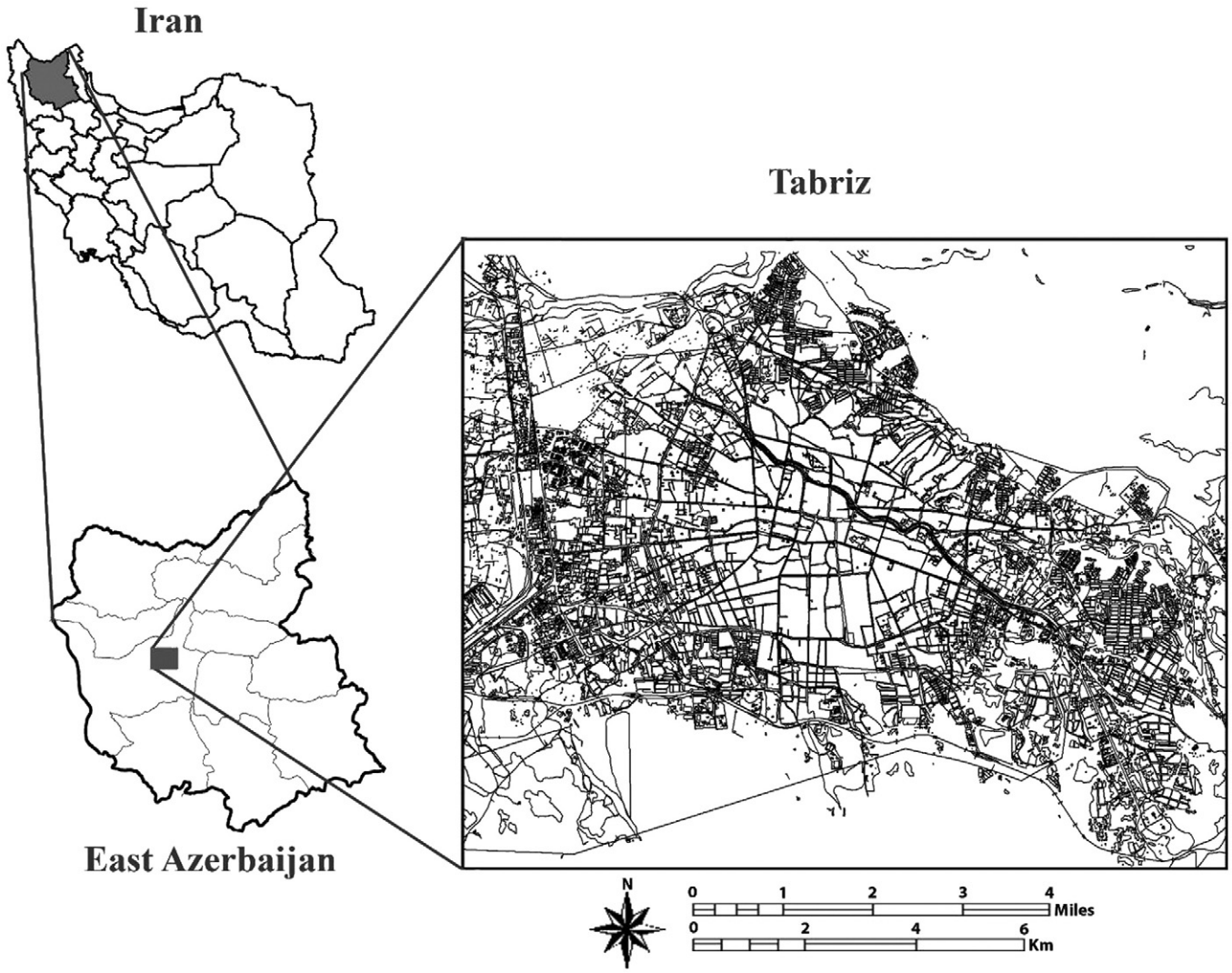

Fig. 1. Map of the study area.

2.3. LST computation and creation of LST–vegetation fraction space

Sobrino et al. (2004) made recommendations for LST retrieval from Landsat 5 TM thermal infrared data based on the comparison of three single-channel LST retrieval methods: the radiative transfer equation using in situ radiosounding data; the mono-window algorithm (Qin et al., 2001); the single-channel algorithm (Jimenes-Munoz & Sobrino, 2003). The above algorithms are as not widely used in urban climate and environmental studies as they deserve, because urban studies are interested in relative LST measurements (Weng, 2009) and their demanding nature. Here, thermal IR bands of Landsat 4, 5 and 7 were used to estimate LSTs according to reference values, calibration data and empirical models widely used in urban surface climate studies as follows.

For Landsat 7, the high gain thermal IR image was transformed to surface temperature in a pixel-based manner in two steps:

First, conversion of DN values to spectral radiance according to reference values in the sensor handbook (Landsat 7 science data user handbook, 2009):

$$L_\lambda = [(L_{\max} - L_{\min}) / (QCal_{\max} - QCal_{\min}) \times QCal] + L_{\min} \quad (2)$$

where: $QCal_{\min} = 1$, $QCal_{\max} = 255$, $QCal = \mathrm{DN}$, $L_{\max}$, $L_{\min}$ = spectral radiance for band 6 at DN 255 and 1 respectively ($\mathrm{W\,m^{-2}\,sr^{-1}\,\mu m^{-1}}$).

Second, transformation of spectral radiance to blackbody temperature by using the following equation:

$$T_b = K_2 / Ln((K_1 / L_\lambda) + 1) \quad (3)$$

where: T_b = effective at-satellite temperature K, K_1 = first calibration constant ($\mathrm{W\,m^{-2}\,sr^{-1}}$) = 666.09, K_2 = second calibration constant (K) = 1282.7, and L_λ = spectral radiance ($\mathrm{W\,m^{-2}\,sr^{-1}\,\mu m^{-1}}$).

For Landsat 5, the second order equation (Malaret et al., 1985) was used to transform DN values to radiant temperature:

$$T_K = 209.831 + 0.334\mathrm{DN} + 0.00133\mathrm{DN}^2. \quad (4)$$

For Landsat 4, a look-up table method was used to transform Landsat 4 thermal IR data (Eastman, 1999), which converted DN values to radiant temperature by referencing values in the table.

The calculated radiant temperatures were corrected for emissivity by using the NDVI. Thresholding the NDVI images into two general vegetation and non-vegetation classes, and assigning emissivity values of 0.95 and 0.92 to them respectively produced emissivity images for each date (Nichol, 1994). Then, land surface temperature was calculated as below (Artis & Carnahan, 1982):

$$T_s = T_b / [1 + (\lambda T_b / \alpha) Ln\varepsilon] \quad (5)$$

where: λ = wavelength of radiance, $a = hc/k$ (h = Planck's constant; c = velocity of light) (k = Boltzmann constant). Because of the importance of vegetation as a temperature controlling factor, the emissivity correction resulted in significant differentiation of classes and increased spatial detail (Nichol, 1996) comparable to those of reflective bands (Fig. 2). Finally, the images were converted to Celsius units.

In order to compare the changes in biophysical parameters in multi-temporal images and examine the relationship between LST and vegetation cover the following method was adopted. It is assumed that with the summertime dry atmospheric conditions, humidity was homogeneous in each image. In order to be able to compare images of different dates, the NDVI and LST values were re-scaled using the method below. Without this step, inter-scene variations in surface state, vegetation phenology and atmospheric conditions (pollution and humidity) might be interpreted as changes in the parameters under study and would affect the correct comparison. This linear operation can also reduce calibration and atmospheric correction errors (Owen et al., 1998). NDVI values for each pixel were scaled between bare soil ($NDVI_0$) and dense vegetation ($NDVI_S$) values acquired within a given scene. The scaled value was calculated by:

$$N^* = (NDVI - NDVI_0) / (NDVI_s - NDVI_0). \quad (7)$$

Using the scaled $NDVI$ (N^*) fractional vegetation cover (Fr) was calculated as:

$$\mathrm{Fr} = N^{*2}. \quad (8)$$

This nonlinear relationship was based on unstressed vegetation condition assumption (Owen et al., 1998). Temperature values were also scaled between the minimum and maximum values. These values were identified in each LST image, and were used to calculate the normalized temperature values:

$$T^* = (T_s - T)_0 / (T_{max} - T_0) \quad (9)$$

where T_S is the land surface temperature for a given pixel, T_0 is the minimum temperature value corresponding to dense vegetation and, T_{max} is the maximum temperature value corresponding to bare soil, all obtained within a given scene. The data from the re-scaled images were plotted as scatterplot of Fr and T^* and showed a triangular pattern (Fig. 3).

2.4. Land use and land cover classification

Preliminary classification by using the maximum likelihood classifier showed some errors. Many single or clustered pixels were

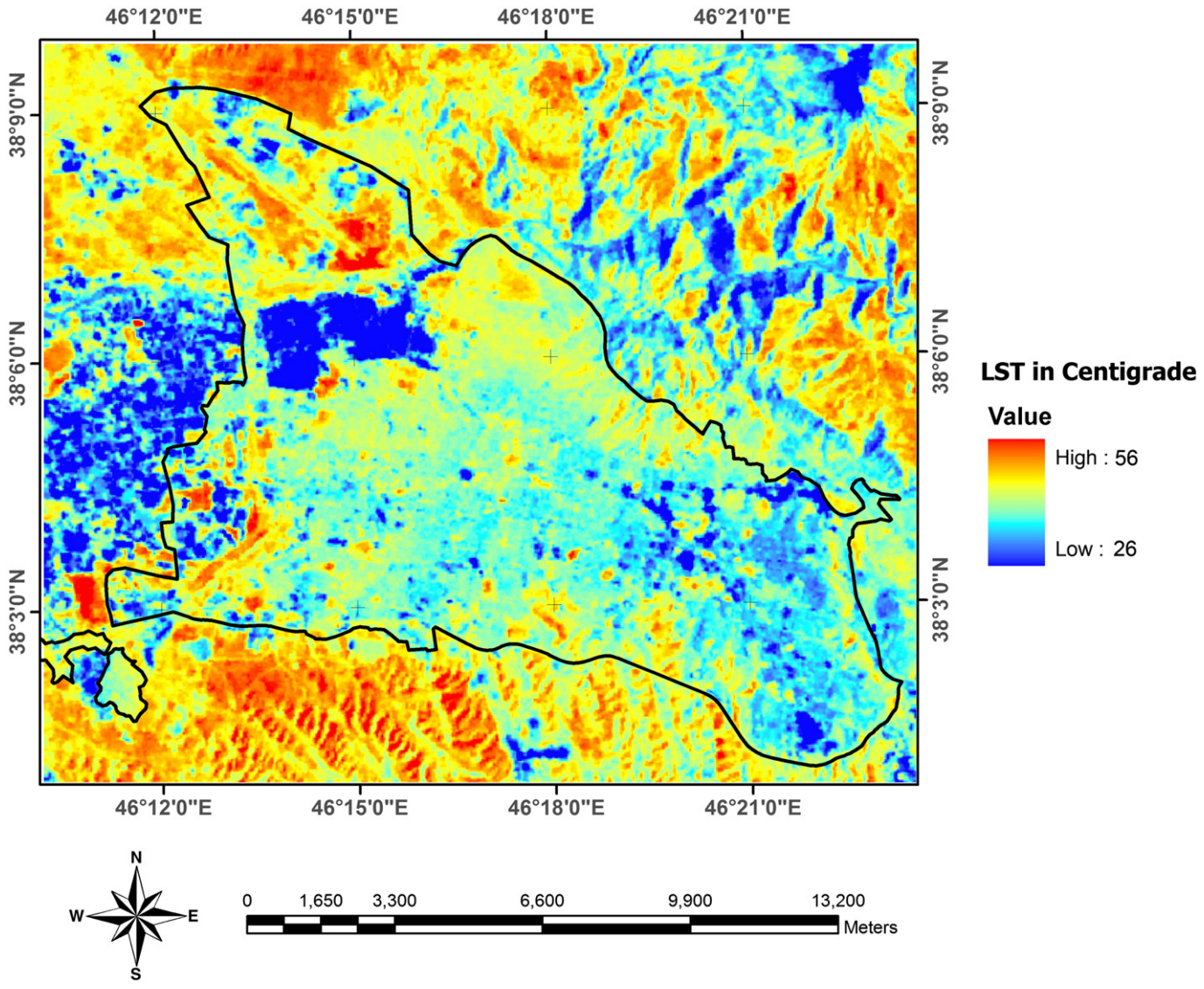

Fig. 2. Emissivity corrected LST in °C (2 August 2001) computed using the method presented in Section 2.3.

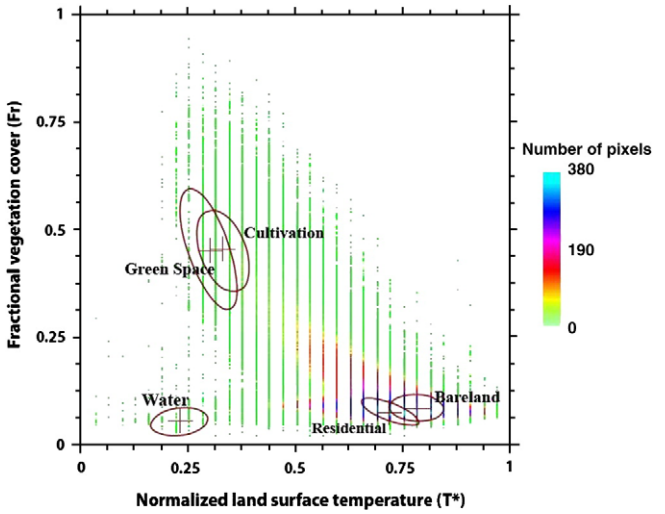

Fig. 3. Scatter plot of normalized surface radiant temperature (T^*) vs. fractional vegetation cover (Fr) from the Landsat 7 image with overlaid target LULC classes, 2 August 2001. Fr and T^* values were calculated according to the Eqs. (7)–(9). The initial range of Fr and T^* (between 0 and 1) was re-scaled to (0–255) due to disk space and processing considerations. The plus signs represent the average value of Fr and $T^*$for the LULC class mentioned on the graph. The surrounding ellipses delineate 1 standard deviation level of Fr and T^* around the mean value showing their variation for each LULC class.

labeled as urban classes in non-urban mountains and urban areas were not correctly classified. Therefore, in order to eliminate this problem, a principal components analysis was used to reduce the possible influence of correlations among the image bands. In addition, data of texture measured by the variance (Haralick et al., 1973) and elevation (Strahler et al., 1978) were also used as additional bands. Application of this method in the classification resulted in accuracy of about 70% in three datasets. A divergence matrix was used to examine the separability of training areas and verify those areas to be used in the classification. For the purpose of accuracy assessment, a confusion matrix was calculated.

By using the LULC classification and surface temperature data, statistical details of each class including the average, maximum and minimum of variance were extracted (Fig. 4). Three separate thermal groups became clear by examining the average values. Water class in all three images was about 5–9° cooler than the other classes. This difference was due to heat transfer capability of water and the transfer of energy as latent heat. The second thermal class (medium

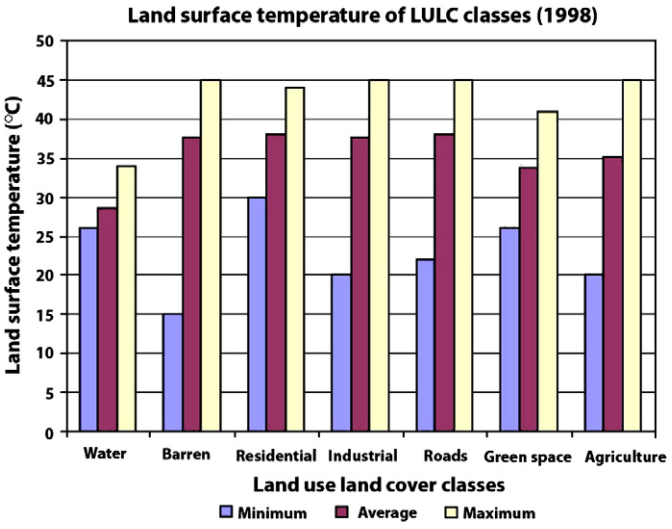

Fig. 4. Bar chart of the surface temperature per LULC class in °C (18 August 1998).

temperature class) included green spaces and cultivation classes. This group showed a 4–5° difference with the hottest group. The cooling mechanism of vegetation was visible as an 'urban cool island' in hot urban areas. Built-up land use classes (residential, commercial and roads) along with bare land class formed the third group, which displayed a high temperature due to the lack of evaporative cooling mechanism and low heat transfer capacity.

The range of values of temperature in each class can be related to the heterogeneity of each class. Cultivation class showed a high range value due to sub-pixel mixing of surface components such as vegetation and dry, bare soil and differences in their thermal properties. For a more detailed study, separation of this class into less general classes may be useful. On the other hand, the residential class, which mostly consisted of impervious surfaces (e.g. asphalt), showed a low range value which was an indicator of the homogeneous construction materials and patterns used in the study area.

2.5. Temporal trajectory

The trajectory analysis was carried out in the TVX space for LULC classes. For this purpose, based on the image classification results, the change image was produced for 1989–1998 period. In the change image, areas with residential change destination were extracted (Fig. 5). The changes of interest were those from bare land, green space, and cultivation to residential. The change image was overlaid on the Fr and T^* images and the mean values of these parameters were extracted and plotted for the starting point (1989) and the end point (1998) and plotted in the TVX space. Fig. 5 shows these changes and the results of pixel trajectory.

3. Results

3.1. Analysis of the LST–vegetation fraction space

The TVX space was formed by plotting the parameter images in an Fr vs. T^* scatterplot (Fig. 4). The overall distribution of the pixels inside the space depicted the typical triangular shape observed by other authors (Lambin & Ehrlich, 1996; Owen et al., 1998; Carlson & Arthur, 2000). Three vertexes of the triangle governed the shape of the triangle reflecting the physical conditions of the area. The upper-left corner corresponded to the pixels representing cool conditions (high Fr and hence low T^*) and lower-right corner was formed by pixels suffering hot conditions (low Fr, high T^*). Fig. 4 demonstrates a clear 'warm edge' defined by the right side of the pixel envelope. The well-known inverse relationship between vegetation indices and LST occurred in the direction of warm edge along the points where a

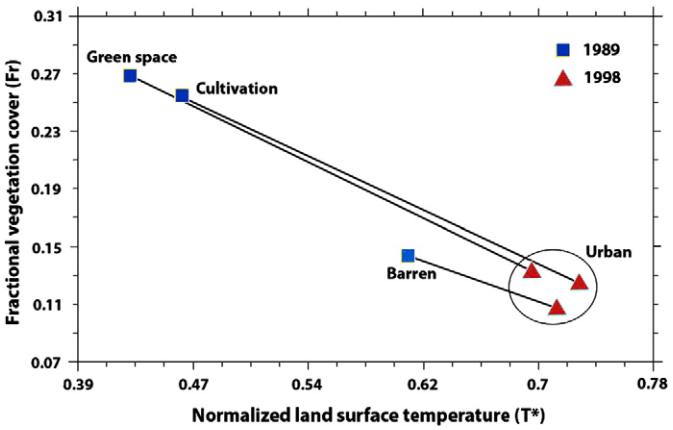

Fig. 5. Change trajectory in the TVX space for the long-term (1989–1998) period (30 June 1989–18 August 1998). The vectors show magnitude of change associated with LULC change from green space, cultivation and barren pixels to urbanized pixels.

decrease in Fr caused an increase in T^*. The majority of the pixels were distributed in this diagonal direction, mainly based on the average transpiration value inside the pixels. However, the third (lower-left) corner which resulted in the triangular distribution had low T^* despite the low Fr, implying that the cooling mechanism for these pixels was mainly evaporation instead of transpiration. Edges of the triangle represent the transition between the two extreme points, without being influenced by the third point. The length and the slope of the edge imply different transition types and could result in different triangles. The space between vertexes and edges was a mixed space (in contrast to the pure vertices), in which the proportion of existing extreme conditions inside a pixel determined the relative location of the pixel. The shape suggested that a full range of different conditions existed in the study area. However, the concentration of the pixels and tendency of the peak values to lower Fr and higher T^* showed that hot conditions were dominant in the study area. The most frequent values were located between ($0.63 < T^* < 0.67$) and ($0.04 < \mathrm{Fr} < 0.08$), which corresponded with the dominant urban and bare land classes (Fig. 4).

To inspect the relationship between the distribution of T^* and Fr values and the target LULC (residential, cultivation, green space, water and bare soils) pixels, spectral characteristics of these classes were extracted. The (+) sign shows the average value, with a surrounding ellipse depicting 1 SD level of T^* and Fr for a given class (Fig. 4). Three distinctive clusters of pixels belonging to different LULC types are apparent, which almost correspond to the vertexes of the triangle. The location of a cluster of pixels belonging to a certain LULC type in the space was related to different cooling mechanisms. Vegetated (cultivated areas, parks and fruit-tree plantations) pixels were concentrated in the upper-left corner and represented cool thermal conditions. This cluster consisted of two LULC types, which largely overlapped and shared common characteristics. A noteworthy point was the position of their average value inside the other class, which showed the difficulty of their separation in this space. The green-space pixels ($0.3 < \mathrm{Fr} < 0.63$) and ($0.23 < T^* < 0.35$) mainly corresponded to two major sub-classes; fruit-tree plantations surrounding the city (and some patches remaining inside the city) and ornamental trees in recreational centers and public parks. The green-space class showed the highest Fr variation with relatively low T^* variations, which showed itself in vertical orientation of the ellipse (Fig. 4). The diverse Fr of this class was due to a different plantation architecture of recreational parks and fruit trees; the former occupied the upper parts of the ellipse while the latter occupied the lower parts. In the case of the recreational parks, trees, shrubs and grasses represented a multi-level greening and resulted in the exposure of green and cool substrate where the trees were not dense and, therefore, occupying cool and green (i.e. upper) parts of the ellipse. In contrast, the lower part of the ellipse was related to fruit-tree orchards (in some cases functioning as recreational centers as well) exposing a dry, tree shadowed and relatively hot substrate because the surface vegetation was removed to save water consumed by weeds. The exposed hot substrate of the fruit-tree class raised the aggregate surface temperature inside a pixel sharply as the trees became sparse, but sub-pixel shading mitigated this effect. The slope of this ellipse could be attributed to the inverse relationship between Fr and surface temperature. The cultivated pixels were generally warmer than the green-space pixels because they consisted of less dense surface coverage. They also exhibited less vegetation fraction variations ($0.23 < \mathrm{Fr} < 0.53$) while showing a slightly higher temperature variation ($0.25 < T^* < 0.39$). These pixels were mainly located in the western fringe of the city. The considerable Fr variability for this class could be attributed to the properties of different types of agricultural products cultivated and some uncultivated patches covered with weeds. This wide range of Fr resulted in relatively large temperature variability.

The second cluster of pixels occupied the lower-right corner demonstrating hot conditions. The two classes in this cluster (urban and bare land) overlap to some extent but less than the first cluster. The location of this cluster near to the peak value of distribution implied that the majority of pixels were those largely affected by urbanization or belonged to a bare natural background. Small variation of Fr ($00.2 < \mathrm{Fr} < 0.11$) showed that the green component inside these pixels of this cluster was not very significant. This was due to the overall design of the city and the sparse vegetation of natural landscape. These two classes demonstrated homogeneous pixels and showed low temperature variation due to a uniform landscape. Brick and concrete were the major construction materials, but asphalt surfaces were more evident as they covered most of the roads and rooftops. The sensor did not view vertical surfaces due to the high altitude of the satellite and relatively low height of the buildings. This condition also made the shadowing effect insignificant in creating variability in T^*. The urban class was expected to show higher variability due to different stages and phases of urban development when it gradually expanded to green areas inside or around the city. However, because the urbanization in these areas occurred at the expense of irrigated green space and started by removing the green space, semi-developed and under development urbanized pixels exposed bare soil, which shared similar characteristics with urbanized pixels, and variability remained low. The temperature variation of bare grounds could be attributed to hillside shadowing. Very sparse vegetation, except for the spots where water was found, made evapotranspiration an insignificant factor in cooling the surface temperature. Bare pixels were also found inside the city in pre-development pixels where vegetation cover was left without irrigation.

A few pixels associated with an artificial water body inside a recreational center in the southwestern part of the city, and wet lands belonging mainly to the cultivation class formed the third corner of the triangle. High thermal capacity, and transfer of energy through latent heat allowed the water pixels to maintain low temperature despite the lack of Fr. Due to the circulation of water, the water body was expected to represent the most homogeneous class in terms of its thermal variability. In fact, the water body showed relatively high variability, which could be related to the contribution of surrounding hotter pixels especially in the edges of the water body.

The position of a cluster of pixels belonging to a certain LULC class may be related to the human manipulation in the natural landscape leading to different physical conditions. The semi-arid landscape of the area belonged to the hot conditions. The cool conditions were achieved by planting vegetation, mainly along the lines of traditional design on this hot natural background. Hot conditions were the result of new development, through which new materials changed the surface energy budget. The implication of this issue on design practice could be either to use large classes of vegetated surfaces such as large parks, or to increase green component inside each pixel to decrease aggregate surface temperature. Based on the observations in the TVX space, it seems that the latter seems more practical, which would shift the urban class away from bare land towards better conditions. The planning recommendations are only based on the analysis of the broad LULC classes. It should be considered that there are several other factors other than the amount of green component that can affect the success of planning projects. For example, as mentioned before different architecture of the green class could result in different surface temperature patterns.

3.2. Temporal dynamics of the LST–vegetation fraction space

3.2.1. Temporal trajectory

Changes in biophysical conditions in each pixel under urbanization could be traced in the Fr/T^* space in multi-temporal studies. The approach used here has some differences to the methods used by others in similar studies, as we used LULC classes to assess the effect of certain types of LULC alteration, instead of geographic subsets, to compare different development styles, as used by Carlson and Arthur (2000) and Owen et al. (1998).

In order to illustrate the thermal effects of certain types of LULC change the pixel trajectory was performed. The trajectory exhibited a migration of pixels from cool and green to hot and bare conditions due to urbanization between 1989 and 1998 (Fig. 5). The most frequent changes were in the green-space class. These areas showed a notable increase in surface temperature ($\Delta T^* = 0.27$) with a decrease in Fr. The bare land class experienced the smallest changes because it was in the similar thermal cluster as the built-up class. A noteworthy point is the general migration trend of pixels undergoing urbanization from cool to hot conditions. This trend was due to large vegetation loss caused by the replacement of fruit-tree plantation and green spaces with impervious urbanized pixels. This conversion affected green-space class (i.e. orchards, fruit-tree sites and ornamental trees) substantially because it followed a large path in the space and faced considerable alteration in the surface climate conditions (Fig. 5). These areas were mostly located in once fringe areas of the city, and were later changed to residential areas at the expense of cooling trees. The second class showing significant change was agriculture (Fig. 5). This class was affected by urbanization mainly in the western parts of the city (Fig. 6). Change path from bare land to urbanization was the abundant type of change (Fig. 6), while its change path in the TVX space was less significant compared to green space and cultivation classes (Fig. 5). As previously observed by Owen et al. (1998) and Carlson and Arthur (2000), pixels undergoing urbanization converged, and tended to concentrate in the lower right (hot condition) corner, and in the last stages of development, they became indistinguishable as they completely lose their initial characteristics (Fig. 5). In this semi-arid region, the latest steps occurred very quickly as the vegetation cover was maintained by irrigation and quickly changed to natural bare lands after being abandoned.

3.2.2. Uncertainty in the TVX space dynamics

As observed previously, urbanization stimulated pixel migration in the form of vectors in the TVX space (Fig. 5). Generally, the length of change vector can be interpreted as the magnitude of the change. However, in fact, in addition to information about real surface alterations, these change vectors included some components of noise resulting from natural variations such as differences in illumination, atmospheric and surface conditions due to different image acquisition times. Therefore, it can be concluded that the vectors in Fig. 5 were composed of signal and noise. In order to address the uncertainty included in the assessment of the urbanization effect, the noise component should be estimated. This was carried out here by identifying the areas that did not undergo any LULC changes and then these No-Change areas were used as control points to assess the uncertainty involved. Ideally, if the vectors were only being controlled by LULC changes, it would be expected that the magnitude of the change vector for the No-Change areas to be equal to zero, but in reality, above-mentioned noise factors could affect the pixels and result in values above zero. Our first premise was that the magnitude of the change vector in the No-Change areas was due to factors other than the changes in LULC type (noise component). The second premise was the assumption that the inter-scene variation (noise factor) affects both Change and No-Change classes of certain LULC type by the same amount. Therefore, the amount of noise can be extracted from No-change classes and be used to separate noise component from change vector. These two premises were the basis for adopting the following methodology. In addition, we hypothesized that the noise effect is not homogeneous but is class-dependant.

By using LULC classification maps and excluding cloud coverage areas, change maps of target change types were produced for the 1989–98 and 1998–2001 periods (Figs. 6 and 7). From the change maps, unchanged

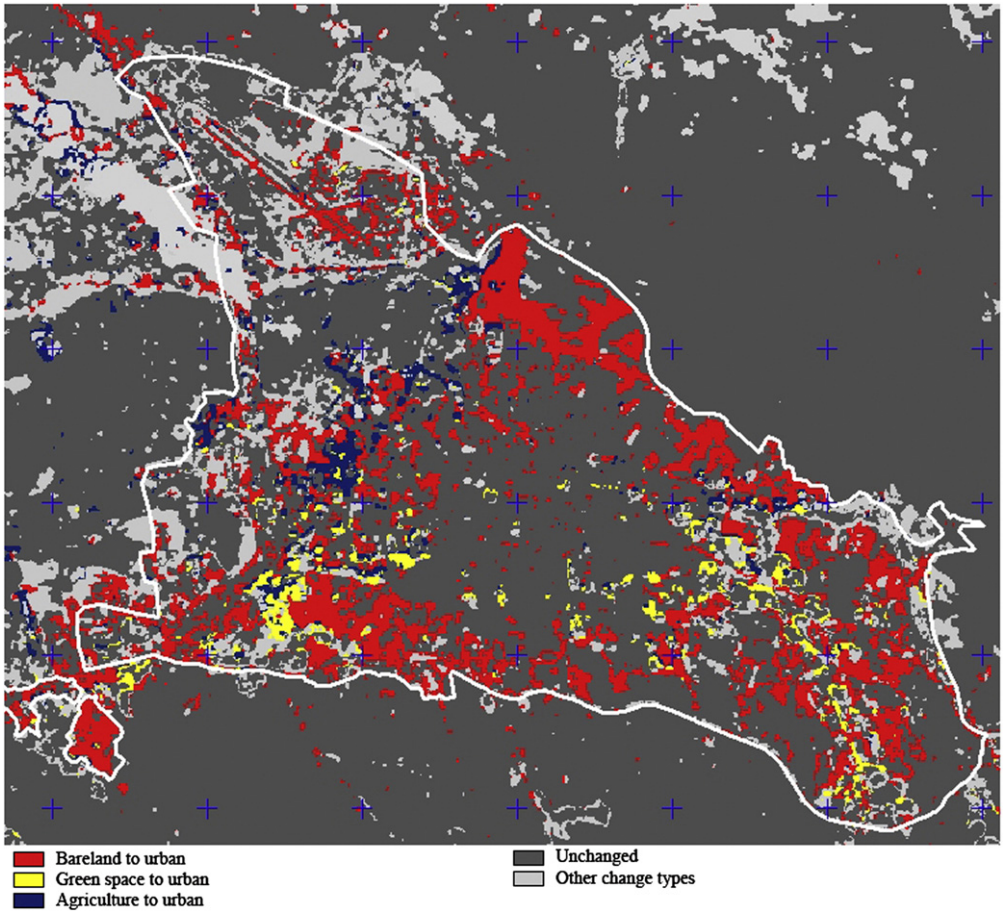

Fig. 6. Change map for the 1989–1998 period (30 June 1989–18 August 1998). The change map highlights the pixels changed from barren, green space and agriculture to urban.

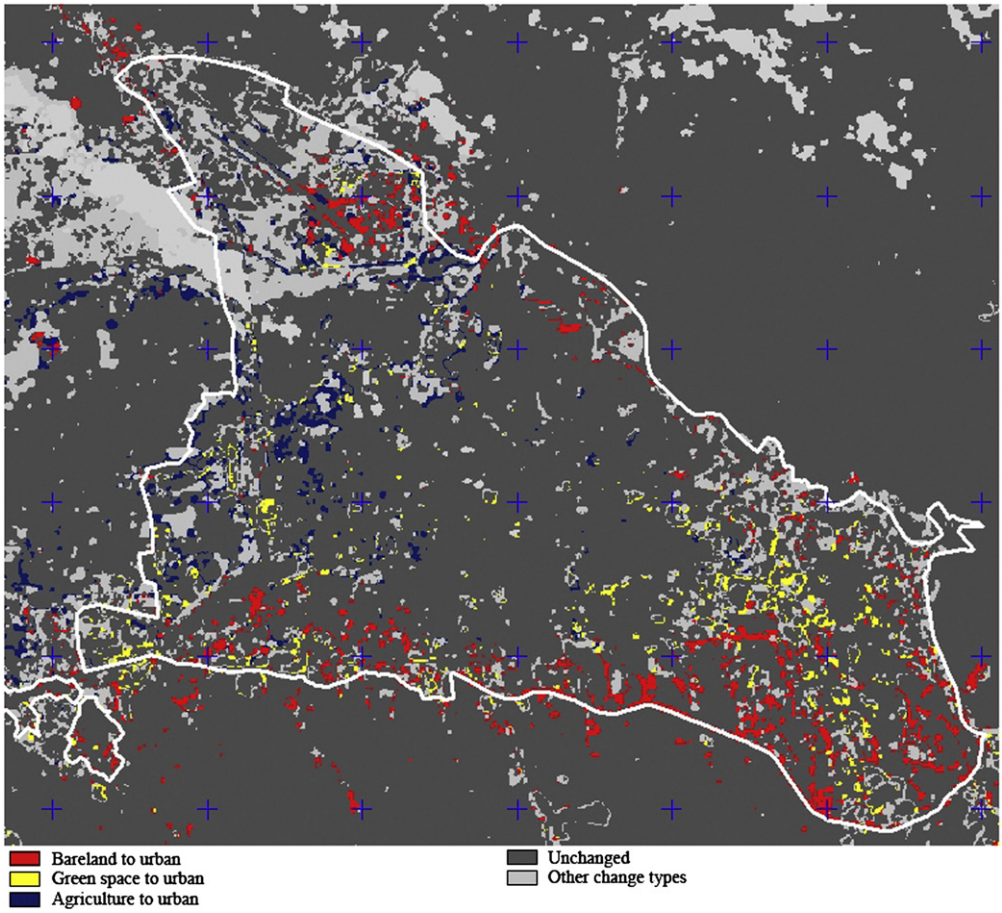

Fig. 7. Change map for the 1998–2001 period (18 August 1998–2 August 2001). The change map highlights the pixels changed from barren, green space and agriculture to urban.

areas for bare land, agriculture, and green space for the two periods were identified as the change from these classes to urban were addressed in the trajectory analysis. From the No-Change areas in 1989, 1998 and 2001 images, average values of Fr and T^* for bare land, agriculture and green-space target classes were extracted separately. Owen et al. (1998) used an average value of all unchanged pixels as the control point. In another study, Carlson and Arthur (2000) used the average value of the whole images as the control point in the TVX space. Here, we used average values for each individual classes involved in the analysis. Using the average values of Fr and T^* for the starting and end point of the two periods (1989–1998 and 1998–2001) a change vector was computed for each No-change class. The magnitude of these change vectors computed for each No-Change type (barren–barren, agricultural–agricultural and green space–green space) were regarded as the threshold values for separation of Change from No-Change for a particular class. A change vector was also computed for each change class using the average values of Fr and T^*. The threshold and change values are shown in Table 1 for 1989–1998 period and in Table 2 for 1998–2001 period. The magnitude of the threshold vectors for No-Change classes in Table 1 were less than the magnitude of the average change vector for change classes implying relatively low uncertainty in this long-term period.

In contrast, according to Table 2, the magnitude of the threshold vector computed for the three No-Change classes (barren, urban and green space) exceeds the magnitude of the average vector of the change class (barren–urban, agricultural–urban, and green space–urban) for the 1998–2001 short-term period. This means that the majority of the pixels in these changed areas probably did not undergo significant changes but were considered as changed by the trajectory analysis.

To demonstrate the uncertainty involved in the estimation of the effects of the target LULC changes on temperature and greenness using the trajectory for each pixel, a change vector was computed for each pixel (Figs. 8 and 9) and used in the following analysis. Standard

Table 1
The statistics for the changes to urban land use between 1989–1998 period.

LULC class		Magnitude of change vector[a]	Population SD (individual vectors)
1989	1998		
Barren	Barren	20.30[b]	12.80
Barren	Urban	28.93	16.19
Green space	Green space	56.47[b]	26.06
Green space	Urban	79.27	37.03
Agriculture	Agriculture	72.02[b]	36.94
Agriculture	Urban	78.40	46.77

[a] The magnitude of change vectors was calculated using the beginning and end values of Fr and T^* averaged inside LULC classes.
[b] These values were used as the threshold values in the uncertainty analysis.

Table 2
The statistics for the changes to urban land use between 1998–2001 period.

LULC class		Magnitude of the change vector[a]	Population SD (individual vectors)
1998	2001		
Barren	Barren	25.01[b]	12.53
Barren	Urban	18.24	8.51
Green space	Green space	35.15[b]	21.42
Green space	Urban	34.32	19.34
Agriculture	Agriculture	47.99[b]	33.32
Agriculture	Urban	34.50	24.45

[a] The magnitude of change vectors was calculated using the beginning and end values of Fr and T^* averaged inside LULC classes.
[b] These values were used as the threshold values in the uncertainty analysis.

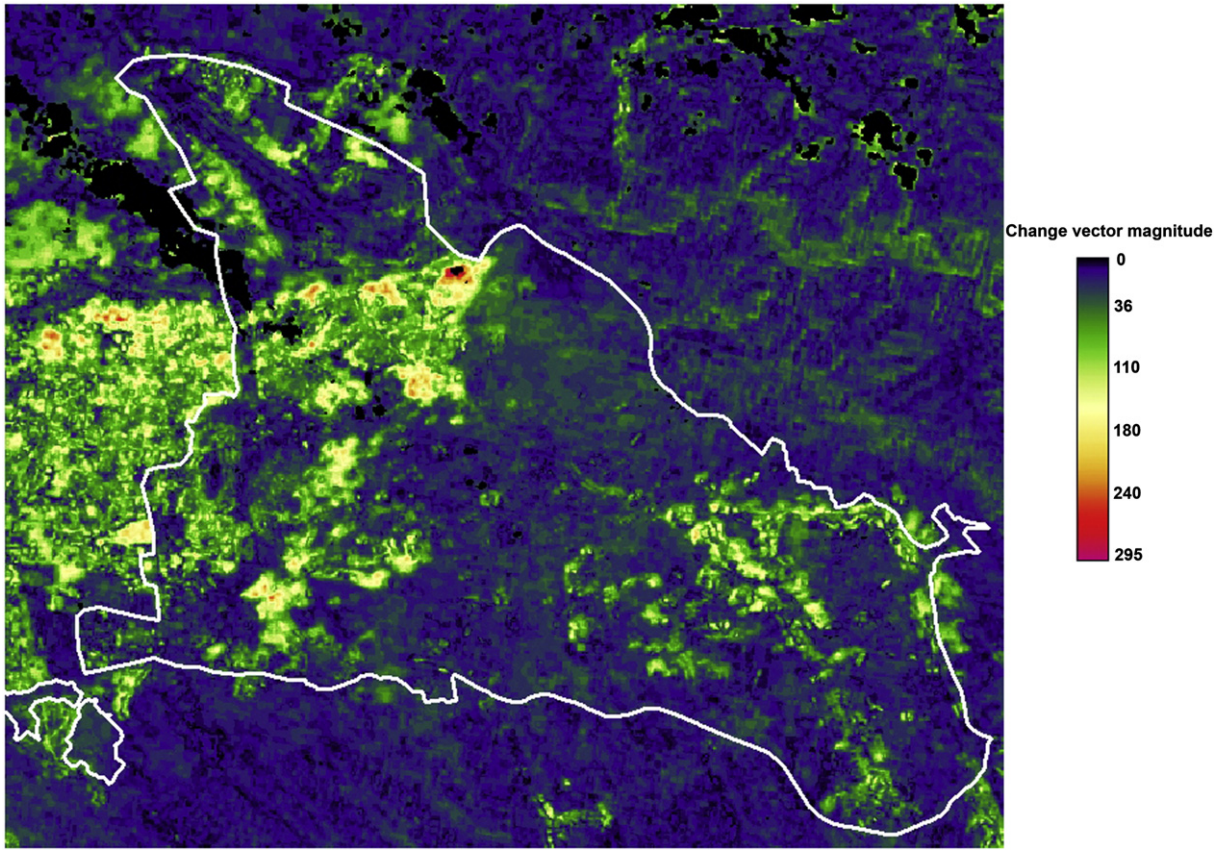

Fig. 8. Change magnitude map for the long-term (1989–1998) period (30 June 1989–18 August 1998). The change vectors were computed for each pixel based on their initial (1989) and final (1998) values of Fr and *T** in the TVX space.

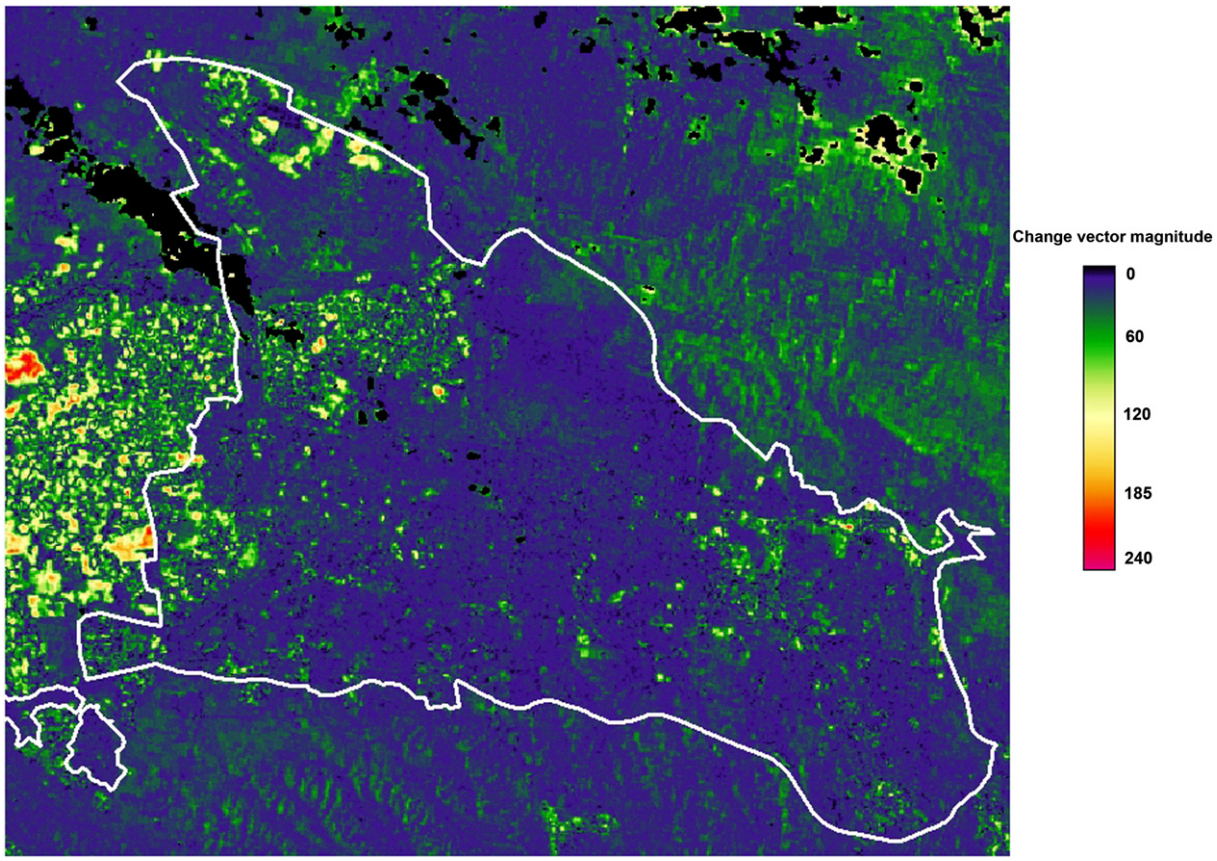

Fig. 9. Change magnitude map for the short-term (1998–2001) period (18 August 1998–2 August 2001). The change vectors were computed for each pixel based on their initial (1998) and final (2001) values of Fr and *T** in the TVX space.

deviation of the change vectors for all Change and No-Change classes was computed using the change vector images and is shown in Tables 1 and 2. The SD values for the 1989–1998 period showed large dispersion of vector magnitudes, which could be related to the uncertainty involved. In contrast, the SD values of the 1989–98 period showed little variation possibly due to the shorter period of the change. The comparison of the SD values of threshold and change vectors shows that the long-term changes were significant. The SD value of threshold vectors for both periods is close to each other and supports the idea that they are related to noise component due to the inter-scene natural variations. Tables 1 and 2 show that more pixels were probably considered incorrectly as changed for the shorter

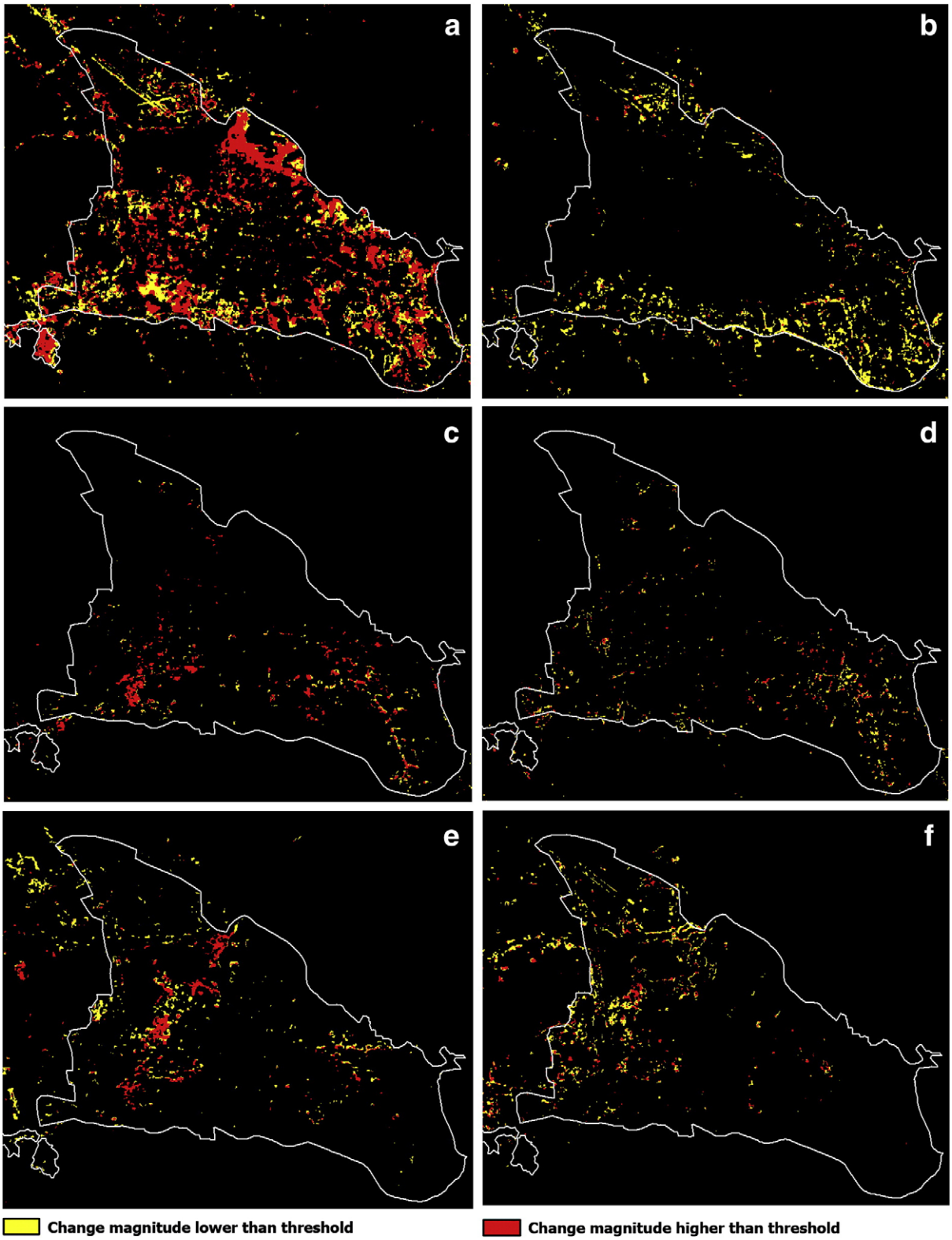

Fig. 10. Changed and unchanged areas for the 1989–1998 period (a, c, d) and for 1998–2001 period (b, d, f). a, b) Bare land to urban; c, d) Green space to urban; and e, f) Agriculture to urban.

period of 1998–2001. It could be concluded from these results that the LULC changes depicted more significant effects for the long-term (1989–1998) period as compared to the short-term (1998–2001) period in the TVX space. The majority of the short-term changes could be due to natural variations, which may be attributed to vegetation phenology, different growth seasons, farming style and image acquisition times.

Fig. 10 shows the uncertainty analysis of the TVX for the both periods by applying the threshold values. These images were produced by applying the threshold values from Tables 1 and 2 to the change vectors for changes from bare land, green space and agriculture to urban classes addressed in the TVX space. The change vector magnitudes for the pixel positions less than the mentioned threshold values for each class were labeled as No-Change in the image space. Fig. 10 shows the areas with real change areas, as well as no-change areas, which due to uncertainty were considered as changed areas. In some cases, the results showed that the majority of the changes were really the effect of the noise component (e.g. 10b and 10f). The examination of the images suggests that the uncertainty was dependant on the LULC change type. For example, the change from bare land to urban LULC class involved more uncertainty than the other change types probably because they belonged to the same cluster and shared similar characteristics (Fig. 10a). The results imply that although an effort had been made to reduce the natural variability of the images and to increase comparability by means of normalization, there was still some uncertainty involved in the results and therefore all the changes could not be considered as real changes. There is a need to consider the effect of the uncertainty involved in the interpretation of the results. The class-dependant nature of the uncertainty prompts for the need to address this issue for individual classes. The results also imply that using an average value of the whole scene as the control point, as used in other studies, was not especially efficient in the study area. In addition, the second method of establishing the control point by averaging a certain class (e.g. agriculture) could not fully address the uncertainty of all class because the uncertainty showed a class-dependant nature.

4. Discussion and conclusions

In this paper, we have examined the spatial and temporal dynamics of LST in relation to LULC change in the TVX space by using Landsat thermal IR and reflective data. Results showed that, if applied over relatively long periods, the adopted methodology might be applied to detect and monitor urban expansion and to trace the changes in biophysical parameters such as NDVI and LST due to LULC changes.

The construction of TVX space by normalizing the land surface temperature and vegetation index data provided comparability between temperature and vegetation datasets of different dates in multi-temporal studies of the urban environment. The TVX space is useful in providing a view of the relationship between LST, NDVI, and LULC classes. This space is also useful in monitoring changes in these parameters and their interplay, as observed in pixel migration. The magnitude and the direction of the movement are defined by the type of change.

The analysis of the distribution of pixels in the TVX space showed that dominant environmental conditions in the study area were hot and dry. This was observed by the association between the distribution peak and the urbanized and barren pixels in hot–dry corner of the TVX space. Traditional human surface alteration created the cool–green edge by irrigated plantations inside the old city and its peripherals and cool–wet edge by creating water bodies. This created different surface climatic conditions, which resulted in the typical triangular distribution in this semi-arid environment. Recent developments have changed these conditions by vast LULC changes, alterations in surface conditions and introduction of new materials. In order to study these effects, a temporal analysis of the TVX space was carried out.

The temporal analysis of the TVX space showed that urbanization resulted in the migration of pixels from cool to hot surface conditions, which is consistent with the observations by other authors (e.g., Owen et al., 1998; Carlson and Arthur, 2000). The extent of pixel migration implied the effect of urbanization in deterioration of environmental quality in the form of changes in surface thermal conditions in the urban areas. The larger path, followed by the green-space pixels in the TVX space as they changed to urbanized pixels, showed that LULC change from green space to urban caused the largest change in surface temperature conditions. Our results showed that in the late stages of urbanization, affected pixels tended to converge and entirely lose their initial characteristics in the TVX space. In contrast with Carlson and Arthur (2000), this study employed a different approach in the trajectory analysis by using original pixel size instead of aggregated pixels. In addition, we used LULC classes instead of geographical subsets as the unit of analysis.

These modifications in the methodology allowed us to investigate the effect of specific LULC change type on LST and to assess the uncertainty in the TVX space. The analysis of the uncertainty involved in the temporal analysis showed that the method used to create a normalized TVX space did not remove the effect of inter-scene variability. There were a certain number of unchanged pixels mistakenly regarded as changed pixels. Our results showed that the amount of uncertainty was class-dependent. This finding suggested that the selection of an average of Fr and T^* for the whole scene as control point could not fully remove the inter-scene variability. In addition, the selection of an un-altered patch of land as control points was not very effective as well due to the same class-dependent nature of uncertainty in the space. The method developed here can be used to remove uncertainty by selection of multiple control points from each LULC classes. The next step in the analysis of uncertainty could be the use of spectral mixture analysis to assess the effect of different compositions of LULC inside the pixels in the migration of pixels and the uncertainty involved. It seems that spectral mixture analysis could be promising in gaining better insight to the mixed TVX space and its internal composition and by providing information on changes in surface climatic conditions (e.g., Weng & Lu, 2009).

The comparison of long-term changes against short-term changes also had implications for this research. The noise component showed more or less comparable effects on both periods. This supports the assumption in our method to consider the magnitude of no-change vectors as the noise component to separate it from the change vector. On the other hand, it showed that the noise component should be addressed for both long-term and short-term changes. The importance of this issue becomes more critical for the short-term period as the majority of the observed change could be due to the effect of noise. This allows us to separate the real change component from the noise component instead of regarding the whole change as insignificant for the short-term period.

A possible application of the TVX space and the analysis carried out here could be the assessment of the consequences of current and future LULC changes associated with urbanization on the surface thermal environment of a city. In the case of the Tabriz urban area, the planned or unplanned changes resulted in the alteration of the cooler surface condition established by traditional designs to hotter ones. This trend was observed by the diagonal migration of the pixels to the hotter corner of the triangular envelope inside the TVX space. The initial condition of migrated pixels was observed as the amount of Fr and type of LULC and associated surface temperature in the TVX space. This observation has the potential to assist informed LULC planning decisions to control changes in surface characteristics in order to modify surface climate by establishing the conditions close to initial ones for each pixel. According to Fig. 5, vegetation could serve as a good remedy for the adverse warming surfaces, which is embraced by

the traditional urban designs. The increase in the fraction of vegetated surface inside a pixel could stop the current migration trend and stimulate the migration of the pixels in the opposite direction in the TVX space. Nevertheless, in case of the green-space classes, it was observed that the variations in the structure and design of the green space could result in slightly different surface thermal conditions. The multi-level design of the recreational parks created cooler surfaces than the orchards. In addition, the expansion of the city in barren lands could cause less surface temperature alterations as the urbanized and barren pixels showed very close characteristics in the TVX space.

References

Artis, D. A., & Carnahan, W. H. (1982). Survey of emissivity variability in thermography of urban areas. *Remote Sensing of Environment*, *12*, 313−329.

Carlson, T. N. (2007). An overview of the so-called "Triangle Method" for estimating surface evapotranspiration and soil moisture from satellite imagery. *Sensors*, *7*, 1612−1629.

Carlson, T. N., & Arthur, S. T. (2000). The impact of land use — land cover changes due to urbanization on surface microclimate and hydrology: A satellite perspective. *Global and Planetary Change*, *25*, 49−65.

Carlson, T. N., & Sanchez-Azofeifa, G. A. (1999). Satellite remote sensing of land use changes in and around San José, Costa Rica. *Remote Sensing of Environment*, *70*(3), 247−256.

Carlson, T. N., Gillies, R. R., & Perry, E. M. (1994). A method to make use of thermal infrared temperature and NDVI measurements to infer surface water content and fractional vegetation cover. *Remote Sensing Reviews*, *9*, 161−173.

Chen, X. L., Zhao, H. M., Li, P. X., & Yin, Z. Y. (2006). Remote sensing image-based analysis of the relationship between urban heat island and land use/cover changes. *Remote Sensing of Environment*, *104*(2), 133−146.

Dousset, B., & Gourmelon, F. (2003). Satellite multi-sensor data analysis of urban surface temperature and land cover. *ISPRS Journal of Photogrammetry and Remote Sensing*, *58*, 43−54.

Eastman, R. J. (1999). *Idrisi guide to GIS and image processing.* Clark University.

Gallo, K. P., & Tarpley, J. D. (1996). The comparison of vegetation index and surface temperature composites for urban heat island analysis. *International Journal of Remote sensing*, *17*, 3071−3076.

Gillies, R. R., Carlson, T. N., Cui, J., Kustas, W. P., & Humes, K. S. (1997). A verification of the 'triangle' method for obtaining surface soil water content and energy fluxes from remote measurements of the normalized difference vegetation index (NDVI) and surface temperature. *International Journal of Remote Sensing*, *18*, 3145−3166.

Goward, S. N., Xue, Y., & Czajkowski, K. P. (2002). Evaluating land surface moisture conditions from the remotely sensed temperature/vegetation index measurements: An exploration with the simplified biosphere model. *Remote Sensing of Environment*, *79*, 225−242.

Haralick, R., Shanmugan, K., & Dinstein, I. (1973). Textural features for image classification. *IEEE Transactions on Systems, Man and Cybernetics*, *3*, 610−621.

Iranian Census Center (2007). *Iranian cities population.*

Jiang, L., & Islam, S. (2001). Estimation of surface evaporation map over southern Great Plains using remote sensing data. *Water Resources Research*, *37*(2), 329−340.

Jimenes-Munoz, J. C., & Sobrino, J. A. (2003). A generalized single-channel method for retrieving land surface temperature from remote sensing data. *Journal of Geophysical Research*, *108*. doi:10.1029/2003JD003480

Kustas, W. P., Norman, J. M., Anderson, M. C., & French, A. N. (2003). Estimating subpixel surface temperatures and energy fluxes from the vegetation index-radiometric temperature relationship. *Remote sensing of Environment*, *85*, 429−440.

Lambin, F. F., & Ehrlich, D. (1996). The surface temperature–vegetation index space for land use and land cover change analysis. *International Journal of Remote Sensing*, *17*, 463−487.

Landsat 7 science data user handbook. Available online: http://landsathandbook.gsfc.nasa.gov/handbook.html. Last accessed July 15, 2009.

Malaret, E., Bartolocci, L. A., Lozano, D. F., Anuta, P. E., & McGillem, C. P. (1985). Landsat 4 and Landsat 5 thematic mapper data quality analysis. *Photogrammetric Engineering and Remote Sensing*, *51*, 1407−1416.

Moran, M. S., Clarke, T. R., Inoue, Y., & Vidal, A. (1994). Estimating crop water deficit using the relation between surface–air temperature and spectral vegetation index. *Remote Sensing of Environment*, *49*, 246−263.

Nemani, R. R., & Running, S. W. (1989). Estimation of Regional Surface Resistance to Evapotranspiration from NDVI and Thermal-IR AVHRR Data. *Journal of Applied Meteorology*, *28*, 276−284.

Nichol, J. E. (1994). A GIS-based approach to microclimate monitoring in Singapore's high-rise housing estates. *Photogrammetric Engineering and Remote Sensing*, *60*, 1225−1232.

Nichol, J. E. (1996). High-resolution surface temperature patterns related to urban morphology in a tropical city: A satellite-based study. *Journal of Applied Meteorology*, *35*, 135−146.

Nichol, J. E. (2005). Remote sensing of urban heat islands by day and night. *Photogrammetric Engineering and Remote Sensing*, *71*, 613−623.

Nishida, K., Nemani, R. R., Glassy, J. M., & Running, S. W. (2003). Development of an evapotranspiration index from Aqua/MODIS for monitoring surface moisture status. *IEEE Transactions on Geoscience and Remote Sensing*, *41*(2), 493−501.

Owen, T. W., Carlson, T. N., & Gillies, R. R. (1998). Assessment of satellite remotely-sensed land cover parameters in quantitatively describing the climatic effect of urbanization. *International Journal of Remote sensing*, *19*, 1663−1681.

Pongracz, R., Bartholy, J., & Dezso, Z. (2006). Remotely sensed thermal information applied to urban climate analysis. *Advance in Space Research*, *37*, 2191−2196.

Price, J. C. (1990). Using spatial context in satellite data to infer regional scale evapotranspiration. *IEEE Transactions on Geoscience and Remote Sensing*, *28*, 940−948.

Qin, Z., Karnielli, A., & Berliner, P. (2001). A mono-window algorithm for retrieving alnd surface temperature from Landsat TM data and its application to the Israel–Egypt border region. *International Journal of Remote Sensing*, *22*(18), 3719−3746.

Quattrochi, D. A., & Luvall, J. C. (2004). *Thermal remote sensing in land surface processes.* CRC Press 440 pp.

Rao, P. K. (1972). Remote sensing of urban heat islands from an environmental satellite. *Bulletin of the American Meteorological Society*, *53*, 647−648.

Ridd, M. K. (1995). Exploring a V–I–S _vegetation–impervious surface–soil. model for urban ecosystem analysis through remote sensing: Comparative anatomy for cities. *International Journal of Remote Sensing*, *16*, 2165−2185.

Sobrino, J. A., Jimenez-Munoz, J. C., & Paolini, L. (2004). Land surface temperature retrieval from Landsat TM 5. *Remote Sensing of Environment*, *90*, 434−440.

Sandholt, I., Rasmussen, K., & Andersen, J. (2002). A simple interpretation of the surface temperature/vegetation index space for assessment of surface moisture status. *Remote Sensing of Environment*, *79*, 213−224.

Smith, R. C. G., & Choudhury, B. J. (1991). Analysis of normalized difference and surface temperature observations over southeastern Australia. *International Journal of Remote Sensing*, *12*(10), 2021−2044.

Strahler, A. H., Logan, T. L., & Bryant, N. A. (1978). Improving forest cover classification from Landsat by incorporating topographic information. *12th International Symposium on Remote Sensing of Environment, Manila, Philippines* (pp. 927−942).

Streutker, D. R. (2003). Satellite-measured growth of the urban heat island of Houston, TX. *Remote Sensing of Environment*, *85*, 282−289.

Voogt, J. A., & Oke, T. R. (2003). Thermal remote sensing of urban climate. *Remote Sensing of Environment*, *86*, 370−384.

Weng, Q. (2001). A remote sensing-GIS evaluation of urban expansion and its impacts on surface temperature in the Zhujiang delta, China. *International Journal of Remote Sensing*, *22*, 1999−2014.

Weng, Q. (2009). Thermal infrared remote sensing for urban climate and environmental studies: Methods, applications, and trends. *ISPRS Journal of Photogrammetry and Remote Sensing*, *64*(4), 335−344.

Weng, Q., & Lu, D. (2009). Landscape as a continuum: An examination of the urban landscape structures and dynamics of Indianapolis city, 1991–2000. *International Journal of Remote Sensing*, *30*, 2547−2577.

Weng, Q., Lu, D., & Schubring, J. (2004). Estimation of land surface temperature–vegetation abundance relationship for urban heat island studies. *Remote sensing of Environment*, *89*, 467−483.